Electron–Lattice Coupling in Armchair Graphene Nanoribbons

ARTICLE *in* JOURNAL OF PHYSICAL CHEMISTRY LETTERS · OCTOBER 2012

Impact Factor: 7.46 · DOI: 10.1021/jz301247u

THE JOURNAL OF PHYSICAL CHEMISTRY Letters

Letter

pubs.acs.org/JPCL

Electron−Lattice Coupling in Armchair Graphene Nanoribbons

P. H. de Oliveira Neto,* J. F. Teixeira, W. F. da Cunha, R. Gargano, and G. M. e Silva

Institute of Physics, University of Brasilia, Brazil

ABSTRACT: We report the effects of electron−lattice coupling on the charge density distribution study of armchair graphene nanoribbons (GNRs). Here, we perform a theoretical investigation explaining the unexpected electronic density states observed experimentally. By means of a tight-binding approach with electron−lattice coupling, we obtained the same characteristic pattern of charge density along the C−C bonds suggested by both scanning tunneling and transmission electron microscopic measurements. Our results suggest electronic localized states whose sizes are dependent on the GNR width. We also show that our model rescues the quasi-particle charge-transport mechanism in GNRs. The remarkable agreement with experimental evidence allows us to conclude that our model could be, in many aspects, a fundamental tool when it comes to the phenomenological understanding of the charge behavior in this kind of system.

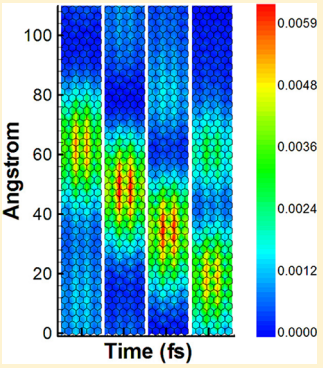

SECTION: Physical Processes in Nanomaterials and Nanostructures

Graphene has been studied extensively due to the fact that it exhibits various remarkable properties as potential replacements for conventional electronic devices such as photodetectors,[1] ballistic semiconductors,[2] and liquid cells.[3] Particularly, due to its unique physical and chemical properties, graphene nanoribbons (GNRs) have been widely investigated. Despite the continued interest in electronic properties of these novel materials, an understanding of the underlying processes involved remains far from satisfactory.

In this Letter, we investigated the charge density distribution pattern and the charge-transport mechanism in armchair GNRs. For this purpose, a tight-binding approach was used in which considered electron−phonon coupling was considered. It is known that this type of interaction, not generally used in tight-binding calculations, is important as far as electronic properties are concerned, especially in the case of low-dimensionality systems, as is the case of conducting polymers.[4,5]

The electronic properties of this novel material are of great importance to charge transport. Of particular importance are the electronic density of states and the charge density. Due to the high electronic density near the Fermi level, it is expected that localization of these states at edges affects the electrical properties of GNRs. However, the pattern of charge density distribution remains controversial. Recently, by means of an atomic-scale scanning tunneling microscopy, a characteristic charge density pattern along the C−C bonds was observed.[6] Also, a similar result was observed in the high-energy transmission electron microscopic images of monolayer graphene.[7] Analyzing the electronic states, we observe that electrons close to the Fermi level have a wave vector, k_F approximately equal to the distance between the Γ and K points of the Brillouin zone. Both foregoing works suggest a quantum interference periodicity approximately equal to the wavelength λ_F. This quantum interference leads to a characteristic charge density pattern along the C−C bonds. However, a different behavior was expected. In metals, the periodicity of quantum interference observed is $\lambda_F/2$. One would expect the same results for both metals and graphene. In fact, the periodicity of quantum interference is analogous to metals in other carbon-based materials. For example, this pattern of quantum interference leads to an electronic charge density delocalized over the phenyl rings in polyaromatic molecules.[8] Also, the charge localization pattern is related to the transport mechanism in these materials. Through an experimental conductance study in disordered GNRs, evidence was found of nonlinear localized states dependent on the size of the system.[9] By considering the applied model, we obtained the same characteristic pattern of charge density along the C−C bonds achieved by both scanning tunneling and transmission electron microscopic measurements. Also, our results suggest electronic localized states whose sizes are dependent on the GNR width. By means of a dynamical study, we observed the collective behavior of these localized states. This result supports the thesis of charge transport based on the hopping through localized states observed in disordered GNRs.[9] The agreement with experimental data suggests that our model is suitable for treating the charge behavior of these systems.

Using the tight-binding approximation scheme, the Hamiltonian assumes the form

$$H = -\sum_{\langle i,j\rangle,s} (t_{i,j} C_{i,s}^{\dagger} C_{j,s} + \text{H.c.}) + \frac{1}{2}\sum_{\langle i,j\rangle} K(y_{i,j})^2 + \sum_{n} \frac{p_n^2}{2M_c} \quad (1)$$

where $C_{i,s}$ is the annihilation operator of a π-electron with s spin in the ith site and $\langle i,j\rangle$ denotes summing over nearest-neighbor

Received: August 14, 2012
Accepted: October 2, 2012
Published: October 2, 2012

   dx.doi.org/10.1021/jz301247u | J. Phys. Chem. Lett. 2012, 3, 3039−3042

sites. The σ-electrons are treated in a harmonic approximation as in the second term of eq 1. Here, $y_{i,j}$ represents the relative displacement coordinate between neighboring sites. In the kinetic term, p_n is the moment conjugated to the displacement coordinate of each site, and M_c represents the carbon mass. Note that the usual tight-binding does not take into account the movement of the lattice, and therefore, the positions of each carbon are fixed. In order to include the electron−phonon coupling, the hopping integral takes the form $t_{i,j} = \exp(-i\gamma A)[t_0 - \alpha y_{i,j}]$ in first-order approximation, where t_0 is the transfer integral normally used in the tight-binding approach and α is the electron−phonon coupling. The electric field is introduced in terms of a time-dependent vector potential, which is present in the Hamiltonian through a Peierls substitution of the phase factor to the transfer integral. In the hopping term, **A** is the vector potential, with γ defined by $\gamma \equiv ea/(\hbar c)$, a being the lattice constant, c the light velocity, and e the absolute value of electron charge. The relation between the time-dependent vector potential **A** and the electric field **E** is given by $\mathbf{E} = -(1/c)\dot{\mathbf{A}}$. In the self-consistent field scheme, the expected value of the Hamiltonian generates an eigenvalue problem that depends on the $y_{i,j}$ coordinates. In turn, the $y_{i,j}$ coordinates depend on the eigenstates of the electronic problem. Thus, from a set of initial values, we seek self-consistent values of energy, eigenstates, and $y_{i,j}$.[5] The electronic problem is coupled to the lattice problem through the terms

$$B_{i,j} = \sum_{k,s}{}' \psi^*_{k,s}(i)\psi_{k,s}(j) \tag{2}$$

in which $\psi_{k,s}$ are the eigenvectors of H. This sum is taken only over the occupied states. Consider the schematic representation of Figure 1. Note that, in general, each GNR bond has four

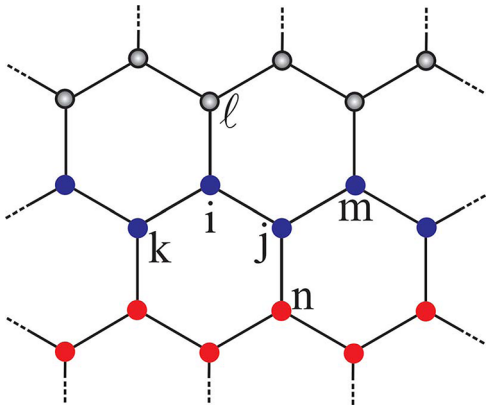

Figure 1. Schematic representation of a GNR.

different neighboring bonds. For this reason, we indexed each site of the lattice with a letter presented in the figure. Thus, each bond is represented by a pair of indexes. The self-consistent state with the degrees of freedom of electrons and phonons is obtained with

$$y_{i,j} = -\frac{\alpha}{K}[B_{i,j} + B^*_{i,j}] \tag{3}$$

for a given bond $\langle i,j\rangle$. Observe that a carbon situated on the boundary of an armchair ribbon can make two or three bonds. In the scope of an Ehrenfest molecular dynamics, we obtain the expected value of the system Lagrangian. The equation of motion used to evolve the lattice is given by

$$M\ddot{y}_{i,j} = -\frac{2K}{3}[(y_{k,i} + y_{l,i} + y_{j,m} + y_{j,n}) - 8y_{i,j}] + \frac{2\alpha}{3}\{e^{i\gamma A}[(B_{k,i} + B_{l,i} + B_{j,m} + B_{j,n}) - 8B_{i,j}] + \text{c.c.}\} \tag{4}$$

The electronic wave functions $\psi_{k,s}$ are the solution to the time-dependent Schrödinger equation solved by the time evolution operator in a base of single-electron eigenstates[10]

$$\psi_{k,i}(t + dt) = \sum_l [\sum_m \phi^*_{l,m}(t)\psi_{k,m}(t)]e^{-(i/\hbar)\varepsilon_l dt}\phi_{l,i}(t) \tag{5}$$

In order to perform the dynamics, first, an initial self-consistent state with the degrees of freedom of electrons and the lattice is prepared. Equations 4 and 5 are solved by discretizing the time variable with a very small value in the electronic time scale.

Concerning the nanoribbon size $M \times N$, the different lines M are represented with different colors in Figure 1. The nanoribbon width is defined by the number of carbons, N, on each line and the length by the amount of lines. In our simulations, nanoribbons of size $64 \times N$ were used with periodic boundary conditions in length with the purpose of reducing the finiteness effect in this direction.

In order to determine the electron−phonon coupling, we carried out a scanning of α values to find the same energy gap from first-principles many-electron Green's function calculations within the GW approximation.[11] The parameters used were $t_0 = 2.7$ eV (as in ref 12), $K = 21$ eV/Å^2, and $\alpha = 5.4$ eV/Å.

We performed simulations with armchair GNRs of $64 \times N$ for $N = 4$, 6, 8, 10, 12, and 14. For better visualization, we present in all figures a region of approximately 40 Å of the lattice. The charge density intensity was represented both in the color pattern (where red means high density) and in the point size (proportional to the density). Each vertical strip represents a nanoribbon of a given width. Also, aiming to simulate the charge density, in all simulation, we submitted the system to a lack of an electron.

Figure 2 presents the charge density of four armchair nanoribbons $N = 4$, 6, 8, and 10. In Figure 2a, we considered the simulation with four sites' widths. Observing the color pattern, we notice greater charge localization on approximately

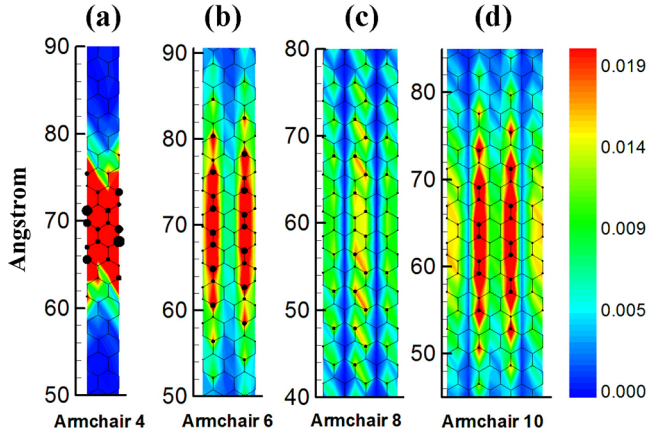

Figure 2. Charge density distributions of N = (a) 4, (b) 6, (c) 8, and (d) 10 armchair GNRs.

dx.doi.org/10.1021/jz301247u | J. Phys. Chem. Lett. 2012, 3, 3039−3042

17 sites localized in the middle of the nanoribbon length tending to pile up at the edge of the nanoribbon width. In the charge distribution of the $N = 6$ nanoribbon in (b), we see, as in Figure 2a, that the charge tends to concentrate in the middle of the nanoribbon. Nevertheless, in this case, the delocalization is increased as the charge density is concentrated along 30 sites. Another important difference between the $N = 4$ and 6 cases is that, in the latter, the charge distributes itself mostly in two separated regions near the edge. Analyzing the point size, we note that inside of the red regions, the charge is considerably uniformly distributed. These results lead us to point out that instead of concentrating in the edges of the armchair nanoribbon, the charge tends to distribute itself along particularly preferred regions. By analyzing the color pattern for the nanoribbon with $N = 8$ in Figure 2c, we note a vertical charge delocalization similar to that obtained in the previous cases ($N = 4$ and 6). However Figure 2c presents three preferred regions of charge localization, represented by the red pattern, interspersed with low-density regions, with the blue signature. Two of those high-density regions are located at the width edge, and the other stands in the middle of the nanoribbon. Also, it allows us to determine a specific pattern for this localization. Taking into account that the charge density values are calculated above the site's position only, the results discussed here suggest that the charge tends to be localized over the carbon−carbon bonds in vertical armchair lines separated by carbon bonds with low charge density. Similar to Figure 2c is the charge density localization pattern presented in Figure 2d, which represents the simulation for the nanoribbon with $N = 10$. In this case, however, we can clearly see the charge localization in two preferred regions, resembling the pattern presented by armchair 6 in Figure 2b. The increase in charge delocalization occurs due to the geometry change in the nanoribbons. The narrower the nanoribbon is, the more important lattice relaxation tends to be, which in turn results in more charge localization. On the other hand, broader nanoribbons tend to present more uniform charge distribution. In this sense, a zoom-in density should be performed in order to provide a better visualization of the results associated to larger nanoribbons. Figure 3 presents the simulation results for armchair nanoribbons of 12 and 14 sites wide. In order to better appreciate the results, the charge density intensity was raised by 40% in the case of nanoribbon 14 in relation to nanoribbon 12. The color pattern makes clear the presence of four separated red regions corresponding to the so-called preferred regions in Figure 3a. Once again the points size suggests that the central regions are the ones associated with higher density. We see that in these middle regions, the charge distribution is nearly uniform. In Figure 3b, we can see that, similarly to Figure 3a, the charge distribution occurs through vertical armchair lines separated by apparently chargeless carbon bonds. Another important issue is related to the similar pattern of charge distribution that nanoribbons belonging to the same "family" (as defined in ref 13) present. Following the same procedure of Yang et al., the following pairs belong to the same family: $N = 4$ and 10, $N = 6$ and 12, and $N = 8$ and 14. For the first pair of nanoribbons ($N = 4$ and 10), we can see that to the smallest nanoribbon is associated with a higher gap energy. This feature is manifested in the figure as the higher level of localization in charge density. In the limit, this is the case of moving away from the graphene regime and approaching the charge-transport mechanism of conducting polymers.[14] This fact is confirmed when we analyze the family composed of $N = 8$ and 14. These nanoribbons have nearly zero energy gap, thus resembling a full graphene sheet. This observed behavior is expected as it is a well-known fact that the metallic conduction, characteristic of very large nanoribbons, is associated with delocalized electronic states whereas conjugated polymers tend to present a charge transport mediated by quasi-particles. Concerning charge distribution, the results reported here are in agreement with recent published experimental evidence,[13] as can be seen in the inset of Figure 3 that presents the same pattern as Figure 3b. The same charge distribution was obtained by scanning tunneling microscopy.[7]

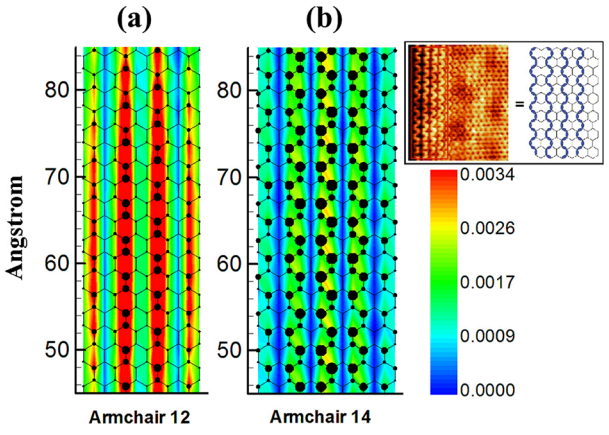

Figure 3. Charge density distribution of N = (a) 12 and (b) 14 armchair GNRs. The inset shows scanning tunneling microscopy from ref 6 and a charge density schematic representation.

In fact the state of charge density localization in GNRs exhibits collective behavior as a quasi-particle. We believe that, for this class of systems, the charge transport is associated with these electronic states. In order to support this, we proceed with a dynamical study in which the nanoribbons are submitted to an external electric field. For this purpose, the electric field applied was 0.65 mV/Å in the direction of the armchair length. The aim was to observe how the charge density responds to this electric field. Specifically, we present the results of a 64 × 12 GNR in four different time steps. Figure 4 presents the charge density spread over the nanoribbon in which each strip represents a different time step. The first strip presents a localized charge density state. As the time runs from the left to the right in the figure, we note that the charge density presents a collective motion toward the direction of the applied field. This can be confirmed by analyzing the successive vertical position of the charge density localization.

We associate the charge density localization in Figure 4 with quasi-particles for both the collective behavior that they present and the fact that the localized state observed in the static simulations previously presented (Figures 2 and 3) remain consistent even with such a intense field applied in the dynamic case. The dynamics presented in Figure 4 is indeed identical to that of an effective charged particle under the action of an electric field. The obtained quasi-particle charge-transport mechanism is in a good qualitative agreement with recent experimental evidence for disordered GNRs.[9]

As a summary, we presented a charge density distribution study of armchair GNRs. By means of a tight-binding model in which the electron−phonon coupling was considered, we found the previously unexplained characteristic pattern of charge density along the C−C bonds obtained by both scanning

dx.doi.org/10.1021/jz301247u | J. Phys. Chem. Lett. 2012, 3, 3039−3042

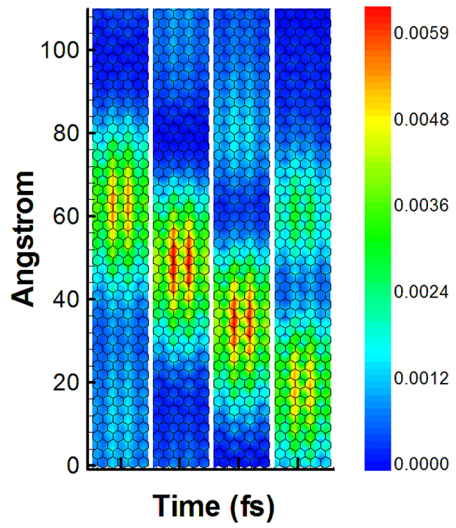

Figure 4. Snapshots of the nanoribbon charge distribution with 4 fs of time difference.

tunneling and transmission electron microscopic measurements. Moreover, this charge pattern is in electronic states whose sizes are dependent on the GNR width. Also, our model allowed us to perform Ehrenfest molecular dynamics to study the charge density behavior under the presence of an external electric field. Our results suggest charge collective behavior as quasi-particles. We believe that these quasi-particles are central structures for the description of charge-transport mechanisms in narrow GNRs.

AUTHOR INFORMATION

Corresponding Author

*E-mail: pedrohenrique@fis.unb.br.

Notes

The authors declare no competing financial interest.

ACKNOWLEDGMENTS

The authors gratefully acknowledge the financial support from the Brazilian Research Councils CNPq, CAPES and FINATEC.

REFERENCES

(1) Echtermeyer, T. J.; Britnell, L.; Jasnos, P. K.; Lombardo, A.; Gorbachev, R. V.; Grigorenko, A. N.; Geim, A. K.; Ferrari, A. C.; Novoselov, K. S. *Nat. Commun.* **2011**, *2*, 458.

(2) Williams, J. R.; Low, T.; Lundstrom, M. S.; Marcus, C. M. *Nat. Nano* **2011**, *6*, 222.

(3) Yuk, J. M.; Park, J.; Ercius, P.; Kim, K.; Hellebusch, D. J.; Crommie, M. F.; Lee, J. Y.; Zettl, A.; Alivisatos, A. P. *Science* **2012**, *336*, 61.

(4) Wehling, T. O.; Grigorenko, I.; Lichtenstein, A. I.; Balatsky, A. V. *Phys. Rev. Lett.* **2008**, *101*, 216803.

(5) Ribeiro, L. A.; Oliveira Neto, P. H.; da Cunha, W. F.; Roncaratti, L. F.; Gargano, R.; da Silva Filho, D.; e Silva, G. M. *J. Chem. Phys.* **2011**, *135*, 224901.

(6) Yang, H.; Mayne, A. J.; Boucherit, M.; Comtet, G.; Dujardin, G.; Kuk, Y. *Nano Lett.* **2010**, *10*, 943.

(7) Girit, Ö. Ç.; Meyer, J. C.; Erni, R.; Rossel, M. D.; Kisielowski, C.; Yang, L.; Park, C.-W.; Crommie, M. F.; Cohen, M. L.; Louie, S. G.; Zettl, A. *Science* **2009**, *323*, 1705.

(8) Repp, J.; Meyer, G.; Paavilainen, S.; Olsson, F. E.; Persson, M. *Science* **2006**, *312*, 1196.

(9) Han, M. Y.; Brant, J. C.; Kim, P. *Phys. Rev. Lett.* **2010**, *104*, 056801.

(10) Oliveira Neto, P. H.; da Cunha, W. F.; Roncaratti, L. F.; Gargano, R.; e Silva, G. M. *Chem. Phys. Lett.* **2010**, *493*, 283.

(11) Hedin, L. *Phys. Rev.* **1965**, *139*, A796.

(12) Castro Neto, A. H.; Guinea, F.; Peres, N. M. R.; Novoselov, K. S.; Gein, A. K. *Rev. Mod. Phys.* **2009**, *81*, 2009.

(13) Yang, L.; Park, C.-H.; Son, Y.-W.; Cohen, M. L.; Louie, S. G. *Phys. Rev. Lett.* **2007**, *99*, 186801.

(14) de Oliveira Neto, P. H.; da Cunha, W. F.; e Silva, G. M. *Europhys. Lett.* **2009**, *88*, 67006.